



# Biocompatibility of titanium from the viewpoint of its surface

Hanawa, Takao

---

**(Citation)**

Science and Technology of Advanced Materials, 23(1):457-472

**(Issue Date)**

2022-12-31

**(Resource Type)**

journal article

**(Version)**

Version of Record

**(Rights)**

© 2022 The Author(s). Published by National Institute for Materials Science in partnership with Taylor & Francis Group.

This is an Open Access article distributed under the terms of the Creative Commons Attribution License (<http://creativecommons.org/licenses/by/4.0/>), which permits...

**(URL)**

<https://hdl.handle.net/20.500.14094/0100476316>





## Biocompatibility of titanium from the viewpoint of its surface

Takao Hanawa

To cite this article: Takao Hanawa (2022) Biocompatibility of titanium from the viewpoint of its surface, Science and Technology of Advanced Materials, 23:1, 457-472, DOI: [10.1080/14686996.2022.2106156](https://doi.org/10.1080/14686996.2022.2106156)

To link to this article: <https://doi.org/10.1080/14686996.2022.2106156>



© 2022 The Author(s). Published by National Institute for Materials Science in partnership with Taylor & Francis Group.



Published online: 15 Aug 2022.



Submit your article to this journal [↗](#)



Article views: 294



View related articles [↗](#)



View Crossmark data [↗](#)

# Biocompatibility of titanium from the viewpoint of its surface

Takao Hanawa <sup>a,b,c</sup>

<sup>a</sup>Institute of Biomaterials and Bioengineering, Tokyo Medical and Dental University, Tokyo, Japan;

<sup>b</sup>Center for Advanced Medical Engineering Research and Development, Kobe University, Kobe, Japan;

<sup>c</sup>Division of Materials and Manufacturing Science, Graduate School of Engineering, Osaka University, Osaka, Japan

## ABSTRACT

Among metals, Ti and majority of its alloys exhibit excellent biocompatibility or tissue compatibility. Although their high corrosion resistance is a factor in the biocompatibility of Ti and Ti alloys, it is clear that other factors exist. In this review, the corrosion resistance and passive film of Ti are compared to those of other metallic biomaterials, and their band gap energies,  $E_g$ s, are compared to discuss the role of  $E_g$  in the reactivity with living tissues. From the perspective of the material's surface, it is possible to explain the excellent biocompatibility of Ti by considering the following factors: Ti ions are immediately stabilized not to show toxicity if it is released to body fluids; good balance of positive and negative charges by the dissociation of surface hydroxyl groups on the passive film; low electrostatic force of the passive film inducing a natural adsorption of proteins maintaining their natural conformation; strong property as *n*-type semiconductor; lower band gap energy of the passive film on Ti generating optimal reactivity; and calcium phosphate formation is caused by this reactivity. The results suggest that due to the passive oxide film, the optimal balance between high corrosion resistance and appropriate reactivity of Ti is the predominate solution for the excellent biocompatibility of Ti.

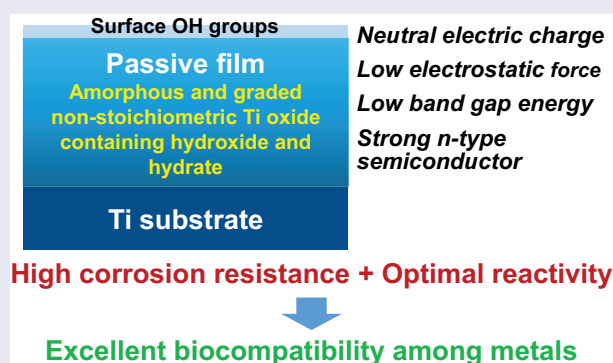
## ARTICLE HISTORY

Received 29 June 2022

Accepted 19 July 2022

## KEYWORDS



Titanium; passive film; corrosion resistance; surface electric charge; electrostatic force; band gap energy; biocompatibility



## 1. Introduction

Commercially pure titanium (CP Ti) and majority of Ti alloys exhibit excellent biocompatibility or tissue compatibility, as demonstrated by a number of studies and clinical findings [1]. However, the dominant mechanism of the biocompatibility of Ti (CP Ti and Ti alloys) is not known, although their high corrosion resistance is a factor. Biological approaches, including interfacial observation between Ti and the surrounding tissue, gene expression of cells on Ti, protein adsorption to Ti, peptide sequence of adsorbed proteins to Ti, bone formation on Ti, soft tissue adhesion to Ti, and bacterial adhesion to Ti, have been utilized to elucidate the mechanism of biocompatibility [1,2]. Ti and zirconia ( $ZrO_2$ ) ceramics are compared as dental implant materials from the perspectives of mechanical property, bone formation, soft tissue adhesion, and antibacterial

property [3]. However, Ti is typically classified as a bioinert material because its bioactivity is significantly less than that of bioactive ceramics [4]. Therefore, the focus of Ti research as a biomaterial has shifted to the improvement of biocompatibility, *i.e.*, the development of surface treatment techniques. To demonstrate the efficacy of surface treatments, the biocompatibility of Ti as a control is typically disregarded: Ti is bioinert. In any case, the principle of Ti's biocompatibility cannot be determined solely through biological approaches, as the biocompatibility's origin lies in the material, particularly its surface. In this review, the corrosion resistance and passive film of Ti are compared to those of other metallic biomaterials, and their band gap energies,  $E_g$ s, are compared to discuss the role of  $E_g$  in the reactivity with living tissues. Figure 1 depicts a summary of the topics covered in this evaluation. Terminology in this review, 'reactivity'

**CONTACT** Takao Hanawa  [hanawa.met@tmd.ac.jp](mailto:hanawa.met@tmd.ac.jp)  Institute of Biomaterials and Bioengineering, Tokyo Medical and Dental University, 2-3-10 Kanda-surugadai, Chiyoda-ku, Tokyo 101-0062, Japan

© 2022 The Author(s). Published by National Institute for Materials Science in partnership with Taylor & Francis Group.

This is an Open Access article distributed under the terms of the Creative Commons Attribution License (<http://creativecommons.org/licenses/by/4.0/>), which permits unrestricted use, distribution, and reproduction in any medium, provided the original work is properly cited.

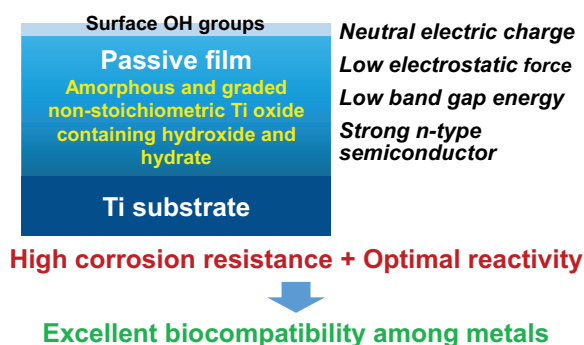


**Figure 1.** Illustration of items reviewed and explained in this review.

includes not only photocatalysis and corrosion but also protein adsorption, calcium phosphate formation, and other reactions occurring at the surfaces of materials.

## 2. Biocompatibility of Ti

Biocompatibility is defined as ‘the ability of a material to perform in a specific application with an appropriate host response [5]’. The biocompatibility of a material is determined by initial and continuous reactions between the material and host body, such as molecule adsorption, protein adsorption, cell adhesion, macrophage activation, tissue formation, bacterial adhesion, and inflammation, etc. In addition, a temporal and spatial hierarchy governs the reaction [2]. When dissolved metal ions from metals in the human body react with biomolecules or cells, disrupting their functions, metal ions have been identified as being toxic to living organisms. To avoid this toxicity, metals used for medical implants must have a high corrosion resistance in the presence of living tissue. Consequently, corrosion resistance is a necessary condition for biocompatibility, as illustrated in Figure 2, but it is not a sufficient condition, as described below.

‘Osseointegration’ is a property unique to Ti among metals [6]. Osseointegration is defined as follows. It is the ‘formation of a direct interface between an implant and bone, with no soft tissue intervening. There is no connective tissue, cartilage, or ligament fibers between the bone and implant surface. Microscopically, the direct contact between bone and implant surface can be confirmed [6]’. This concept, osseointegration, in dental implants generated and accelerated studies on the reaction between hard tissues and Ti, followed by surface treatment studies. Studies on: evaluation of osteoblast calcification; histological evaluation, such as bone formation, bone-contacting rate, and bone bonding strength; and clinical results have demonstrated Ti’s excellent compatibility with hard tissues. Important determinants of hard-tissue compatibility are the adhesion and proliferation of osteogenic cells as a result of the surface morphology (roughness), wettability, and other characteristics. Ti-bone interface reaction has been characterized to demonstrate the significance of surface morphology and wettability for osseointegration [7–9]. Numerous studies on the compatibility of Ti with hard tissues have been conducted, and detailed information is available in the literature [1,2]. In orthopedics, bone screws and bone nails made of Ti alloys typically form calluses and assimilate into bone tissue after long-term implantation, causing the bone to refracture during retrieval [10]. This is due to the fact that Ti alloys are compatible with hard tissues.

## 3. Corrosion behavior of metallic biomaterials

### 3.1. Corrosion resistance of Ti and Ti alloys

Numerous studies confirm the Ti’s superior corrosion resistance in biological environments. CP Ti, Ti–6 aluminum (Al)–4 vanadium (V) alloy, nickel (Ni)–Ti alloy, cobalt (Co)–nickel (Ni)–chromium (Cr)–

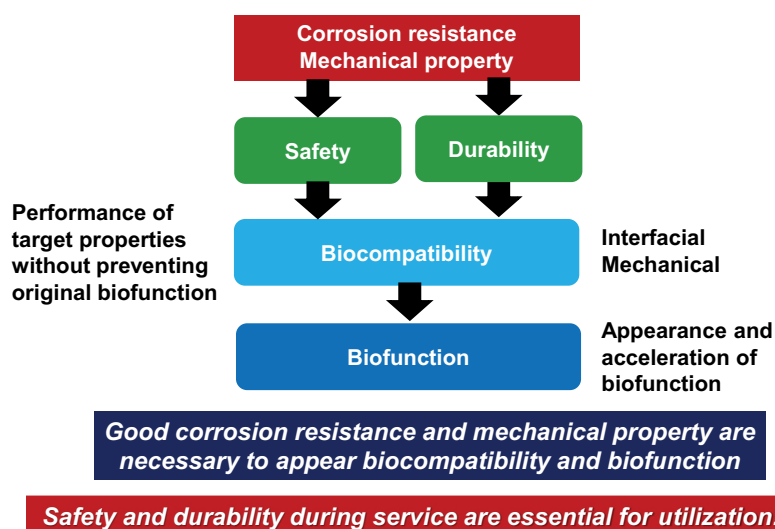


**Figure 2.** Corrosion resistance and mechanical property as necessary condition for the biocompatibility and biofunction.

molybdenum (Mo) alloy, Co–Cr–Mo alloy, type 316 L stainless steel, and pure Ni exhibit the strongest passivation in this order in Hanks' physiological solution at 37°C and 7.4 pH [11]. Afterwards anodic polarization measurements of several orthopedic implant metals and alloys, including type 316 L stainless steel, Co–Cr–Mo alloy (ASTM F-75), Ni–Ti alloy, pure Ni, CP Ti, and Ti–6Al–4V alloy, are performed in Ringer's solution with and without 1% bovine serum albumin [12] and in Ringer's solution and rabbit [13], which demonstrates the excellent corrosion resistance of CP Ti and Ti, as shown in Figure 3. Recent studies [14,15] have produced comparable results. The corrosion behaviors of the aforementioned materials have been thoroughly reviewed [16]. Both CP Ti and Ti–6Al–4V alloy demonstrate much lower passive currents and higher breakdown potentials without pitting in vitro and in vivo.

### 3.2. Ti element released to the surrounding tissues

Despite the high corrosion resistance of Ti, since more than three decades, numerous studies [17–22] have demonstrated that despite the absence of abrasion, a significantly greater quantity of Ti elements is detected in the surrounding tissues when Ti materials are implanted.

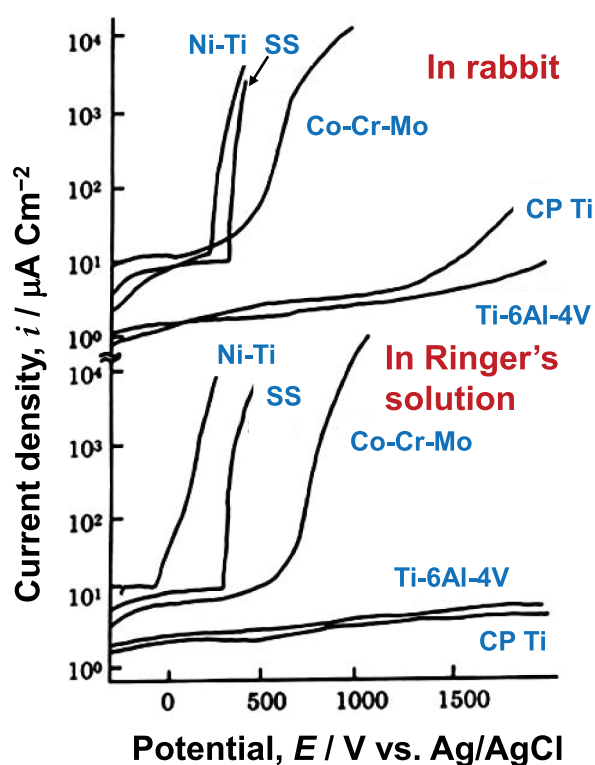


**Figure 3.** Anodic polarization curves of CP Ti, Ti–6Al–4V alloy, Co–Cr–Mo alloy, type 316L stainless steel (SS), and pure Ni in rabbit and Ringer's. Reproduced by permission from [13], copyright [1989, Elsevier].

The effect of amino acids and proteins on the solubility of metals is examined [23,24]. Possible Ti ion dissolution mechanisms are examined from the perspective of the isoelectric point and the electric charge of proteins contained in body fluids [25]. Mo, copper (Cu), Co, and Ni ions are released when pure metal powders are immersed in saline, with or without serum albumin or fibrinogen, but Ti ions are not released and are unaffected by the presence of proteins [26]. In the case of Ti–6Al–4V, Ti and Al ions are released in Hanks' solution containing 2% EDTA, whereas Ti, Al, and V ions are released in Hanks' solution containing 0.05-M sodium citrate [27]. Ni–Ti alloy initially releases more Ni than stainless steel immersed in a medium containing osteoblasts or fibrinogen, but the amount released decreases after two days [22]. As a result, metal ions are released in rabbits in the absence of wear and are detected in the rabbit's tissues, serum, and urine. Fretting corrosion depends on (the charge of) proteins; in the presence of proteins, Ni preferential dissolution increases [25]. Biomolecules may account for the release of metal ions. Although the mechanism for the accelerated release of metal ions in the presence of amino acids and proteins has not been elucidated, an imbalance between partial dissolution and re-precipitation in the passive film may accelerate the release of ions. Therefore, repassivation of a metal influences the release of ions from the metal. During the repassivation of Ti in aqueous solutions, inorganic ions, and proteins accelerated the repassivation of Ti, whereas certain amino acids slowed it [28].

Immunological reactions and the adhesion of macrophages (MΦ) to the surface of an implanted material identify it as a foreign body [29]. MΦ generates active oxygen species,  $H_2O_2$ , which has a much longer lifetime and higher permeability against cell membrane than  $O^{2-}$ .  $H_2O_2$  reaches the surface to which MΦ has adhered, and the Ti surface is hyper-oxidized by  $H_2O_2$  [30,31], which may result in the release of Ti ions.  $H_2O_2$  reacts with the passive film on Ti according to the following equation [31]:  $Ti^{4+} + H_2O_2 \rightarrow Ti^{5+} + OH^- + OH^*$ , where \* represents radical. Dissolution of Ti with active oxygen generated by MΦ has been elucidated adequately [32]. On the other hand, surgical handling during implantation and wear and/or fretting were the leading causes of Ti release [33].

Regardless, despite the detection of Ti element in the surrounding tissues, the toxicity of Ti materials has hardly manifested. In the majority of instances involving the detection of released Ti elements, the chemical states of these elements are obscure. As depicted in Figure 4, dissolved Ti ions combine immediately with hydroxide ions and anions to stabilize the Ti element in the human body and are utilized for the reconstruction of the passive film. Therefore, the possibility of Ti

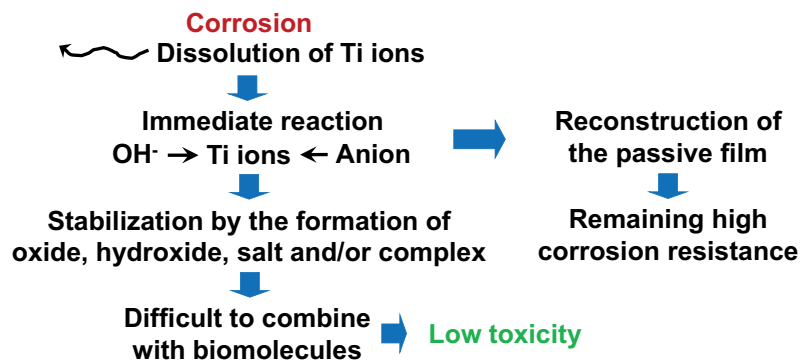


**Figure 4.** Mechanism remaining low toxicity even though Ti is corroded.

surviving as ionic states and combining with biomolecules is extremely low. Consequently, Ti exhibits low toxicity.

### 3.3. Stainless steel

Ti alloys have replaced the majority of stainless steels used for the stems of artificial hip joints and bone fixators due to their lower corrosion resistance. However, stainless steel is still utilized for retrievable internal bone fixators and sternal and bone fixation wires due to its superior torsion property and elongation to fracture. Stainless steels are also utilized for medical and surgical instruments and equipment. For implant materials, type 316 L austenitic stainless steel always used. Adding 2.0–3.0 mass% of Mo, increasing Ni from 8.0–10.0 mass% to 12.0–15.0 mass%, and decreasing carbon (C) to less than 0.030% increases its corrosion resistance [34]. The presence of Mo reduces both the number of nucleations and the size of metastable pits. This is due to the strengthening of bonds in the passive film and the elimination of active pitting sites caused by the formation of molybdates or molybdenum oxyhydroxides [35].

In biological environments, type 316 L stainless steel typically exhibits pitting corrosion due to anodic polarization, as shown in Figure 3. Severe crevice corrosion of spinal rods is observed in the human body [36]. In addition, severe corrosion pitting was observed on sternal wires implanted for over 30 years [37]. Consequently, the corrosion resistance of type 316 L stainless steel is considerably less than that of Ti and Ti alloys.

### 3.4. Co–Cr alloys

Co–Cr alloys show excellent mechanical properties, castability, corrosion resistance, and wear resistance [34]. The absence of crevice and pitting corrosion in Co–Cr alloys is confirmed by anodic polarization in simulated bioliquids [38], and the Co–Cr alloys have a high localized corrosion resistance that is

independent of a small change in composition [39]. Their corrosion resistance is superior to that of stainless steel. Their wear resistance is superior to that of stainless steel, CP Ti, and Ti alloys.

In the field of orthopedics, a cast Co–Cr–Mo alloy known as ‘Vitallium’ (ASTM F75) is utilized for artificial knee joints and artificial hip joints, in particular, the heads. ASTM F79 Co–Cr–Mo alloy is produced by refining the grain of F75 using hot rolling. The F99 alloy has twice the tensile strength and yield strength of the F75 alloy. To improve the workability of Co–Cr–Mo alloy, ASTM F90 as ‘HS25’ or ‘L-605’, used for orthopedic wire, is developed by reducing the C content and adding W and Ni, resulting in a workability of 44% and a strength after working that is more than double that of F75 alloy. ASTM F562 Co–Ni–Cr–Mo alloy as ‘MP35N’ is used in cardiovascular surgery for stents with superior strength, elasticity, and corrosion resistance, and tensile strength exceeding 1600 MPa. This alloy, along with the ASTM F90 alloy, has a high elastic modulus, which makes it advantageous for use as a stent. On the other hand, ASTM F1058 Co–Cr–Ni–Mo–iron (Fe) alloy, also known as ‘Elgiloy’, is utilized for artificial heart springs and aneurysm clips. Co–Cr–Mo alloy is utilized in dentistry for removable partial dentures with clasp, crowns, and bridges [34].

However, Co–Cr alloys can experience metallosis due to the Co release. A 56-year-old female with metal neuropathy and a Co–Cr alloy hip prosthesis developed metallosis. Co and Cr levels in her blood decreased after exchange arthroplasty, and her symptoms improved. Elements containing Co or Cr can cause axonopathy [40]. Cases with pseudotumors typically indicate poorly functioning implants and have significantly higher median metal ion concentrations: median Co levels were found to range from 6.9 to 29.7 µg/L [41]. Co–Cr alloy implant particles were associated with persistent, dose-dependent peri-spine inflammation [42].

The primary cause of the aforementioned metallosis is the release of Co ion. Co ions released from the passive film on the alloys [43–47]. During releasing Co



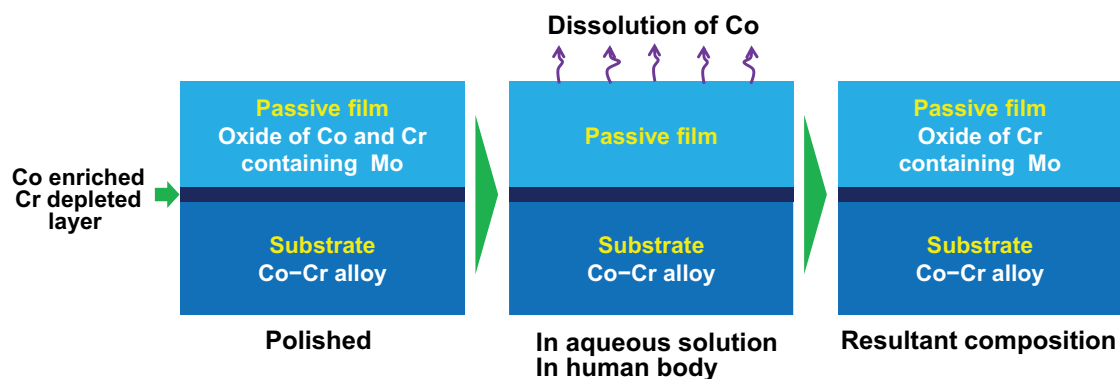


**Figure 5.** Co ions are released from initial passive film in aqueous solutions or the human body and the resultant passive film is Cr oxide containing small amount of Mo.

ions, Cr, Mo, tungsten (W), and Ni are enriched in the passive film, whereas Co is depleted, in accordance with their oxidation and reduction potentials. Figure 5 illustrates this occurrence. Therefore, under wear conditions, Co ions are released repeatedly [48,49], and the amount of Co ions released may be substantial. Therefore, the above clinically observed metallosis is due to the release of Co ions following implantation.

### 3.5. Ni–Ti alloy

Ni–Ti alloys composed of equal amounts of Ni and Ti (49–51 mol%Ni) exhibit exceptional mechanical properties, including shape memory, superelasticity, and damping. The Ni–Ti alloy is utilized for guide wires, stents, orthodontic arch wires, and endodontic files due to its exceptional properties [34].

As stent grafts, Ni–Ti alloys exhibit severe pitting and crevice corrosion. The observed corrosion defects of pitting and irregular shape are precursors to material failure. They weaken the thin wire, resulting in stress cracks and eventual fracture of the stent wire when subjected to circulation pulses [50]. Although the materials chosen for the construction of endovascular grafts appear prudent, the assembly of these biomaterials into various interconnected structures within the device requires further development [51].

### 3.6. Summary of corrosion

Metals with the best corrosion resistance in biological environments are Ti and its alloys. Co–Cr alloys also exhibit good corrosion resistance in the absence of pitting and crevice corrosion; however, the alloys release Co ions in aqueous solution to stabilize the passive film, so Co ions are repeatedly released under wear conditions. Type 316 L stainless steel and Ni–Ti alloy exhibit pitting and crevice corrosion on occasion. Therefore, Ti has the highest corrosion resistance among metals.

## 4. Relationship between corrosion resistance and biocompatibility in Ti

The corrosion resistance of Ti is one of the reasons for its excellent biocompatibility; however, corrosion resistance is not a sufficient condition for biocompatibility. Even gold (Au), the most corrosion-resistant metal, has poor tissue compatibility. Preosteoblasts on Ti and zirconium (Zr) differentiate and calcify more rapidly than those on Au [52]. In addition, the electric plating of platinum (Pt) onto Ti increases corrosion resistance but decreases bone formation because a property of Ti is shielded, thereby preventing bone formation [53]. These results indicate that compatibility with hard tissues is not solely determined by corrosion resistance. In other words, corrosion resistance is a necessary but insufficient condition for biocompatibility; there are other contributing factors.

## 5. The passive film on Ti

### 5.1. Composition and chemical state

Except in environments of reduction, the corrosion process always results in the formation of a reaction film on metallic materials. Passive film is one such reaction film, and its importance for corrosion protection is especially noteworthy. When solubility is extremely low and pores are absent, film adhesion will be strong to the substrate. The film then becomes a passive or corrosion-resistant film. A passive film has a few nanometers of thickness and is transparent. Passive film readily becomes amorphous as a result of the incredibly rapid rate at which it is formed [54,55]. For instance, a film was generated on a Ti metal substrate in approximately 1/100 s. Figure 6 depicts the transient current density following the rupture of the passive film. In 30 ms, the current density approaches zero, indicating that the passive film is reconstructed immediately. Since amorphous films contain few grain boundaries and structural defects, they are resistant to corrosion. However, crystallization decreases corrosion resistance. Thankfully, passive films contain water molecules that promote and preserve amorphousness.

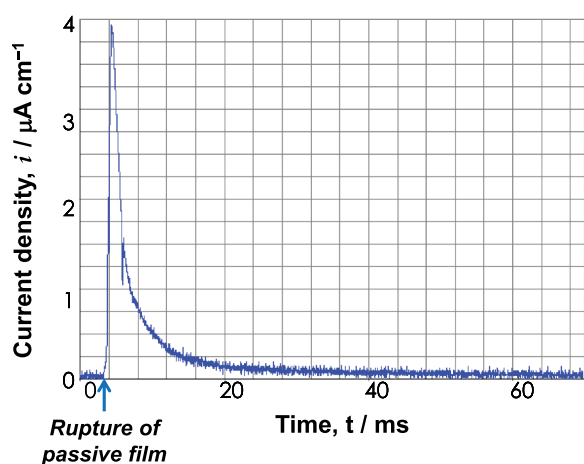


**Figure 6.** Time transient of current density of Ti after rupturing the passive film by abrasion in Hanks' solution at 1 V vs. SCE. Positive current is generated both by ion dissolution and the formation of the passive film.

Metallic Ti naturally form the surface oxide film on itself according to the following equations. In acidic solution, the anodic reactions are:  $\text{Ti} + 2\text{H}_2\text{O} \rightarrow \text{Ti}(\text{OH})_2 + 2\text{H}^+ + 2\text{e}^-$  (oxidation to divalence);  $\text{Ti}(\text{OH})_2 \rightarrow \text{TiO} + \text{H}_2\text{O}$  (dehydration);  $\text{TiO} + \text{H}_2\text{O} \rightarrow \text{TiOOH} + \text{H}^+ + \text{e}^-$  (oxidation to trivalence);  $2\text{TiOOH} \rightarrow \text{Ti}_2\text{O}_3 + \text{H}_2\text{O}$  (dehydration);  $\text{Ti}_2\text{O}_3 + 3\text{H}_2\text{O} \rightarrow 2\text{TiO}(\text{OH})_2 + 2\text{H}^+ + 2\text{e}^-$  (oxidation to tetravalence);  $2\text{TiO}(\text{OH})_2 \rightarrow \text{TiO}_2 + 2\text{H}_2\text{O}$  (dehydration). On the other hand, in neutral and basic solutions, the anodic reactions are:  $\text{Ti} + 2\text{OH}^- \rightarrow \text{Ti}(\text{OH})_2 + 2\text{e}^-$  (oxidation to divalence);  $\text{Ti}(\text{OH})_2 + \text{OH}^- \rightarrow \text{TiOOH}^- + \text{H}_2\text{O}$  (dehydration);  $\text{TiOOH}^- + \text{H}_2\text{O} \rightarrow \text{TiOOH} + \text{e}^-$  (oxidation to trivalence);  $2\text{TiOOH} \rightarrow \text{Ti}_2\text{O}_3 + \text{H}_2\text{O}$  (dehydration);  $\text{Ti}_2\text{O}_3 + 4\text{OH}^- \rightarrow 2\text{TiO}(\text{OH})_2 + \text{H}_2\text{O} + 2\text{e}^-$  (oxidation to tetravalence);  $2\text{TiO}(\text{OH})_2 \rightarrow \text{TiO}_2 + 2\text{H}_2\text{O}$  (dehydration). Since a considerable portion of oxidized Ti stays in  $\text{Ti}^{2+}$  and  $\text{Ti}^{3+}$  in the surface film, the oxidation process may proceed to the end just at the uppermost part of the surface film.

Consequently, when Ti is characterized using X-ray photoelectron spectroscopy (XPS), the Ti 2p spectrum exhibited four doublets according to valence: the metallic state of  $\text{Ti}^0$  and the oxide states of  $\text{Ti}^{2+}$ ,  $\text{Ti}^{3+}$ , and  $\text{Ti}^{4+}$ , as depicted in Figure 7(a) based on previously published data [56,57]. The decomposition spectrum reveals the presence of  $\text{Ti}^{2+}$  oxide within the surface oxide layer; however,  $\text{Ti}^{2+}$  formation is thermodynamically inferior to  $\text{Ti}^{3+}$  formation at the surface [58–60]. As depicted in Figure 7(b), the spectrum of the O 1s region contained three peaks originating from  $\text{O}^{2-}$ , hydroxide or hydroxyl groups,  $\text{OH}^-$ , and hydrate or adsorbed water,  $\text{H}_2\text{O}$  [61]. Concerning the average effective escape depth of photoelectrons as determined by angle-resolved XPS measurements,  $\lambda$  was the average mean free path of Ti 2p and O 1s photoelectrons, and the effective escape depth was estimated as  $\lambda$  times than the sine of the take-off angle [56,62]; was the average mean free path of Ti 2p and O 1s photoelectrons; Figure 8(a) depicts the ratio of the relative oxygen concentration to that of Ti,  $[\text{O}]/[\text{Ti}]$ , versus the average photoelectron escape depth. Oxygen was more abundant in the outer layer of the passive film, while Ti was more abundant in the inner layer.  $[\text{Ti}^{4+}]/([\text{Ti}^{4+}] + [\text{Ti}^{3+}] + [\text{Ti}^{2+}])$ , obtained using the angle-resolved technique, is depicted in Figure 8(b) as the proportion of the integrated intensity of the peak attributed to  $\text{Ti}^{4+}$  relative to all of its oxide states. At small take-off angles, the percentage of  $\text{Ti}^{4+}$  was high, indicating that  $\text{Ti}^{4+}$  was distributed more in the passive film's outer layer than in its inner layer. In addition, the depth profiles of the  $[\text{OH}^-]/[\text{O}^{2-}]$  ratios are depicted in Figure 8(c), which reveals that  $\text{OH}^-$  was more abundant in the passive film's outer layer. Consistent with previous research, it is evident that the passive film on Ti consists primarily of an extremely thin  $\text{TiO}_2$  film with trace amounts of  $\text{Ti}_2\text{O}_3$  and  $\text{TiO}$ , as well as water and hydroxyl groups [55,62,63]. This process of passive film formation has been covered elsewhere [59]. The topmost surface

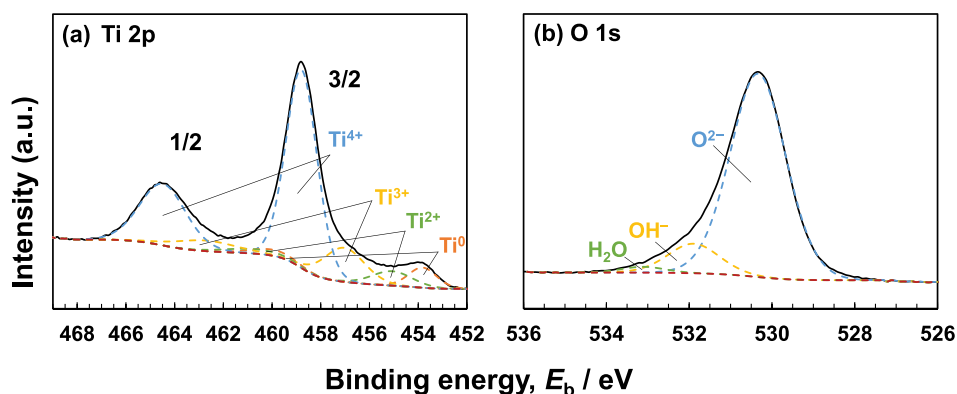


**Figure 7.** Ti 2p (a) and O 1s (b) electron energy region spectra obtained from Ti immersed in pure water for 1 d and their deconvolutions into component peaks [56].



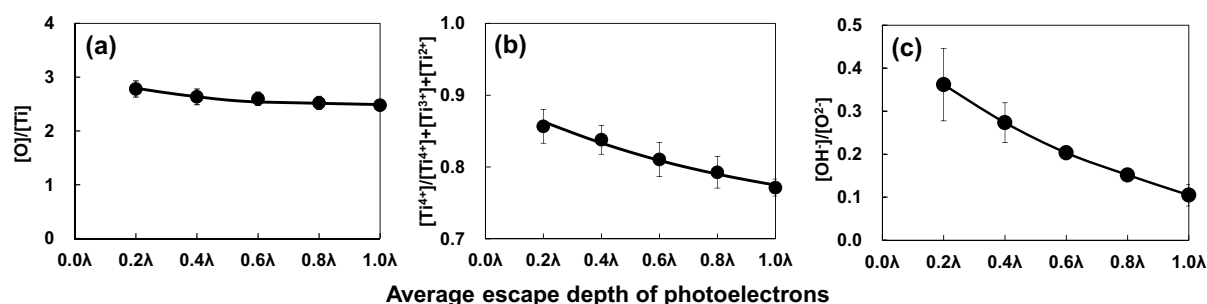


**Figure 8.** The ratios of [O]/[Ti] (a),  $[\text{Ti}^{4+}]/([\text{Ti}^{4+}]+[\text{Ti}^{3+}]+[\text{Ti}^{2+}])$  (b), and  $[\text{OH}^-]/[\text{O}^{2-}]$  (c), plotted against the average escape depth of photoelectrons ( $n = 3$ ) [56]. The angle-resolved technique for XPS was applied to Ti at the photoelectron take-off angles of 12°, 24°, 37°, 53°, and 90°, corresponding to the detection depths of 0.2λ, 0.4λ, 0.6λ, 0.8λ, and 1.0λ, where λ was the photoelectrons' effective mean free path. The effective escape depth was estimated as λ times the sine of the take-off angle. The take-off angle was defined as the angle between the direction of the photoelectron path to the electron spectrometer and the specimen surface.

(~5.0 nm) reveals that the ratio of  $[\text{TiO}_2]/[\text{Ti}_2\text{O}_3]$  is consistent with that of passivation/dissolution of electrochemical activity, and that both the structures of passivation, dissolution are distorted due to the appearance of two different sites of Ti–O and Ti–Ti, with bound water in the topmost surface playing a crucial role in structural disorder [64]. It has been determined that the composition, structure, and chemical state of the passive film are distinct from those of crystalline  $\text{TiO}_2$  ceramics. Therefore, the adsorption kinetics of calcium and phosphate ions differ between passive films on Ti and  $\text{TiO}_2$  ceramics [65].

## 5.2. Property as *n*-type semiconductor

As is common knowledge,  $\text{TiO}_2$  ceramics function as *n*-type semiconductors. How does the passive film on Ti behave as a semiconductor? As shown in Figure 9, the maximum energy of the balance band,  $E_v$ , versus Fermi energy,  $E_F$ , is determined by linearly extrapolating the peak to the baseline [67] (A). The  $E_v$  value of anatase is approximately 0.2 eV greater than that of rutile [66]. In the case of the passive film on Ti, the  $E_v$  are 2.8–2.9 eV in Hanks' solution and 2.8–3.0 eV in saline [68], while that in the polished Ti without polarization is 2.8–2.9 eV; this is a higher value than that for rutile, which was 2.5 eV

[67]. The observed  $E_v$  value of the as-deposited  $\text{TiO}_2$  film was 1.86 eV [67]. Therefore, the  $E_v$  value for the passive film on Ti was greater than the  $E_v$  value for ceramics composed of  $\text{TiO}_2$ . Figure 9 depicts the difference in  $E_v$  versus  $E_F$  between the passive film on Ti and  $\text{TiO}_2$  (B). In other words, the energy between the conduction band's minimum energy,  $E_c$ , and the passive film's  $E_F$  is less than that of  $\text{TiO}_2$ . In addition, as will be explained later, the  $E_g$  of the passive film on Ti is between 2.7 and 2.9 eV, which is significantly less than 3 eV, indicating that the property as an *n*-type semiconductor is much stronger in the passive film on Ti than in the  $\text{TiO}_2$  ceramics.

## 5.3. Dissociation of surface hydroxyl groups – surface electric charge

The interface reaction between Ti and living tissue is governed by the passive film property of Ti. This passive film forms hydroxyl groups on their surfaces due to a reaction with atmospheric moisture [69]. In aqueous solutions, such as body fluid, these hydroxyl groups dissociate to form electric charges [69–71]. At a particular pH, the electric charge becomes zero. It is dependent on the pH of the surrounding solution. This pH is defined as the zero-charge point (p.z.c.) (Figure 10). The p.z.c. is specific to each oxide and

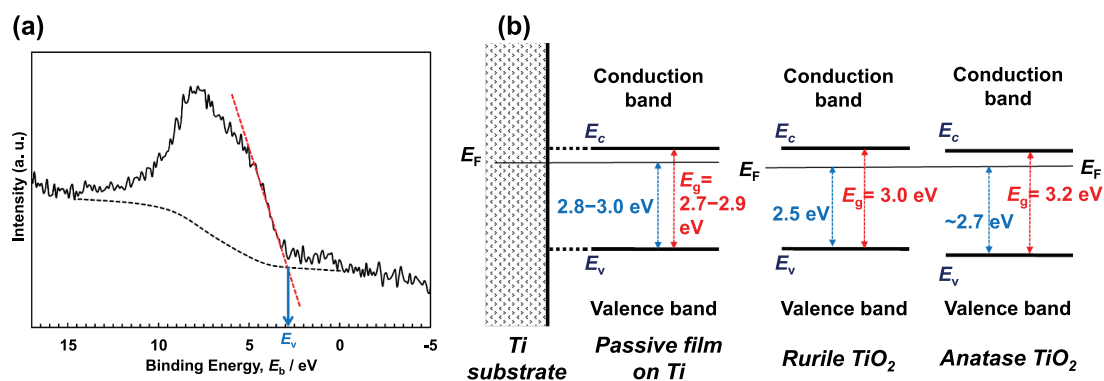


**Figure 9.** (a) Valence band region spectra of Ti after polarization at 0 V in Hanks for 1 h and the determination of the maximum energy of the valence band,  $E_v$  [66]. (b) Relationship among  $E_g$ ,  $E_v$ , and  $E_F$  in the band structures of the passive film on Ti, rutile  $\text{TiO}_2$ , and anatase  $\text{TiO}_2$ .

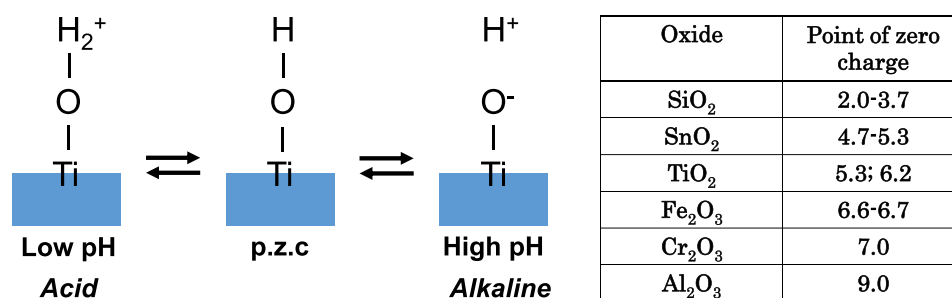


**Figure 10.** Point of zero charge (p.z.c.) of surface hydroxyl groups on TiO<sub>2</sub> and their dissociation in aqueous solutions according to pH. The p.z.c. values of metal oxides are listed in the table.

serves as an indicator of acidic or basic properties (table in Figure 10). In the case of TiO<sub>2</sub>, rutile has a p.z.c. of 5.3 and anatase has a p.z.c. of 6.2 [71]; therefore, TiO<sub>2</sub> demonstrates neither an acidic nor a basic property, but rather an almost neutral property. The surface concentration of hydroxyl groups on TiO<sub>2</sub> is relatively high 4.9–12.5 nm<sup>-2</sup> [70,72]. This concentration or wettability increases when immersed in an aqueous solution. This high concentration promotes the adsorption of proteins, such as integrin and cytokine.

#### 5.4. Dielectric constant – electrostatic force

Since proteins are electrically charged objects, adsorption to a metal surface aggravates the conformation of proteins. The electrostatic force exerted by proteins on a metal surface is determined by the relative permittivity of the passive film; the greater the relative permittivity, the lower the electrostatic force. The relative permittivity of TiO<sub>2</sub> is 82.1, which is significantly greater than that of other oxides and comparable to that of water (80.0) [73]. Consequently, the conformational change of protein adsorbed on TiO<sub>2</sub> may be minimal. On Ti, the fibrinogen adsorption layer is thicker, but the adsorption amount is less than on Au

in aqueous solution [74]. Because Ti is covered by TiO<sub>2</sub> and Au is exposed without surface oxide, the electrostatic force on Ti is small compared to Au. On Ti, the conformational change of proteins is smaller than on Au. Proteins adsorbed on Ti are more natural.

#### 6. Calcium phosphate formation on Ti

Maintaining corrosion resistance, the passive film is macroscopically stable. From a microscopic standpoint, a passive film generally maintains a continuous process of partial dissolution and re-precipitation in the electrolyte [55]. Consequently, the composition and chemical state are affected by the environment. In this way, the surface composition of the passive film is constantly changing in response to its surroundings. Ti and Ti alloys readily form calcium phosphates and sulfite and sulfide in biological environments, particularly under cell culture [75–80]. Recent research [63] has elucidated the initial formation kinetics of calcium phosphate on Ti. First, phosphate ions were incorporated, then calcium ions were incorporated to form calcium phosphate on Ti. Figure 11 demonstrates that calcium and phosphate were incorporated by direct reaction between the Ti

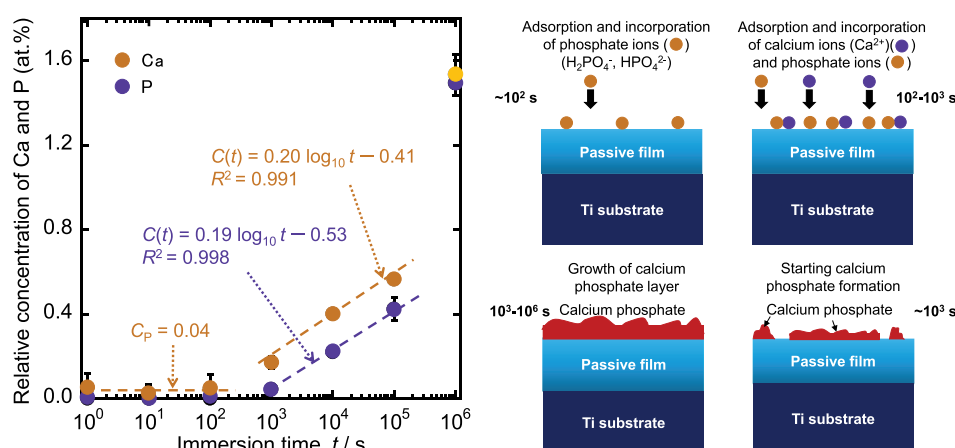


**Figure 11.** Change in the relative concentrations of calcium and phosphorus in the surface layers of Ti immersed in Hanks' solution ( $n=3$ ) and illustration of the formation process of calcium phosphate on Ti in Hanks' solution [63].

substrate and calcium and phosphate ions as calcium and phosphate concentrations increased as immersion time increased from  $10^3$  s to  $10^5$  s. Additionally, calcium and phosphorus are found at the interface between Ti and bone tissue [81–83]. Zr does not form calcium phosphate against Ti, but rather zirconium phosphate. The passive film on Ti is not fully oxidized and is relatively reactive, whereas the passive film on Zr is more stable and protective than that on Ti [84]. The following section clearly explains these phenomena from the perspective of the  $E_g$ . Niobium (Nb) and tantalum (Ta) exhibit properties intermediate to those of Ti and Zr [85]. Electrochemical impedance and photoelectrochemical measurements have characterized the direct interaction of calcium and phosphate ions with the passive film of Ti-6Al-4 V alloy in physiological solutions [86], and calcium phosphate formation on Ti-6Al-4 V alloy is dependent on defects in the passive film [87]. The ability of Ti to form calcium phosphate is therefore one of the reasons for its superior compatibility with hard tissues.

## 7. Band gap energy

### 7.1. $\text{TiO}_2$ and $\text{CaTiO}_3$ ceramics

The optical absorption edge is typically used to evaluate the  $E_g$  between the valence and conduction bands in crystalline  $\text{TiO}_2$  ceramics. It is well known that  $E_g$  determines the reactivity of  $\text{TiO}_2$  ceramics, and numerous efforts have been made to reduce  $E_g$  to

improve their photocatalyst performance [88]. Therefore, the  $E_g$ s of  $\text{TiO}_2$  anatase and rutile are intensively researched for photocatalyst applications. Figure 12 presents a summary of the published data on  $\text{TiO}_2$  ceramics. The  $E_g$  values vary depending on the specimen preparation, which affects oxygen defects and surface morphology.

In the case of anatase,  $3.20 \pm 0.02$  eV for anatase thin film on mica and 3.1–3.2 eV for P25 high-purity fine particle [89], 3.22 eV for pure anatase particle [90], 3.28 eV for anatase and 3.22 eV for anatase high-purity fine particle [91], 3.39 eV for multi-crystal anatase film, 3.51 eV for epitaxial anatase film, and 3.20 eV for bulk anatase [92], 3.15 eV for (001) facet of anatase [93], 3.2 eV for anatase experimented and  $3.25 \pm 0.12$  eV for anatase calculated [94], and 3.26 eV for anatase and 3.20 eV for P25 nanoparticle [95].

In the case of rutile,  $3.08 \pm 0.02$  eV for petaloid rutile [89], 2.96 eV for a pure rutile particle [90], 3.34 eV for multi-crystal rutile, 3.37 eV for an epitaxial rutile film, 3.03 eV for bulk rutile [92], 3.04 eV for the (100) facet of rutile [93], 3.05 eV for rutile experimented and  $3.25 \pm 0.12$  eV for rutile calculated [92], and 3.05 eV for rutile [95].

In the case of brookite, 3.15–3.25 eV was experimentally determined and 3.25 eV is calculated [94].

In the case of amorphous and unidentified  $\text{TiO}_2$  crystals, 3.15–3.25 eV for porous  $\text{TiO}_2$  and 3.22–3.26 eV for nanometer-sized  $\text{TiO}_2$  [91], 3.48 eV for stoichiometric  $\text{TiO}_2$  and 3.35 eV for non-stoichiometric  $\text{TiO}_2$  [96], 3.42–3.45 eV for non-stoichiometric  $\text{TiO}_x$

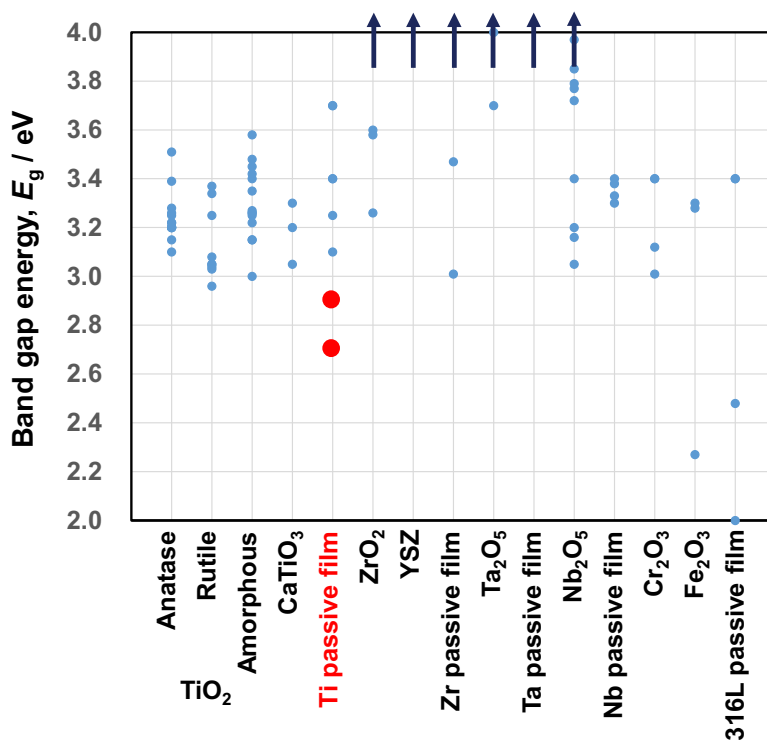


**Figure 12.** Band gap energies of various oxides and passive films on metals. This figure was originally drawn based on band gap energy data in published papers. The band gap energy of the passive film on Ti in simulated bioliquids (red circles) is relatively low, which may contribute to the reactivity of Ti.

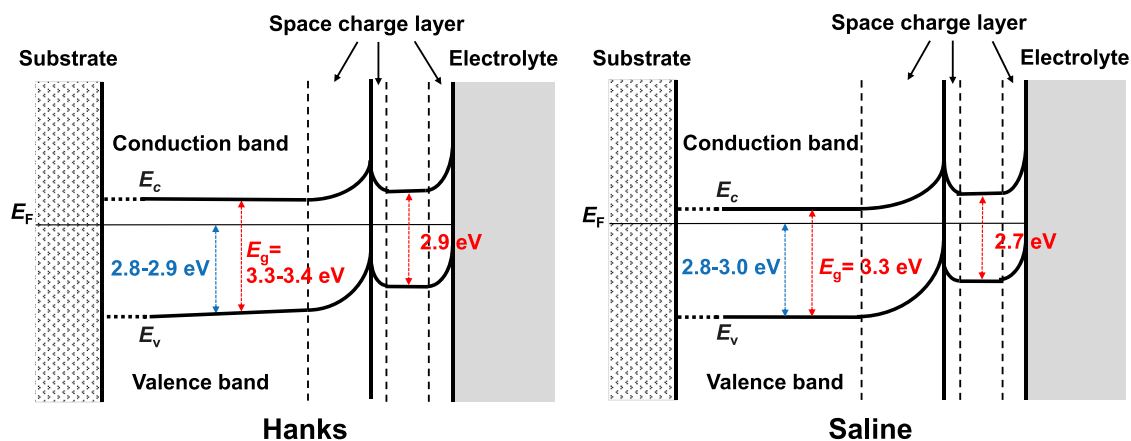


**Figure 13.** Electronic band structures of passive films formed on Ti in Hanks' solution and saline [68].

[97], 3.15–3.27 eV for TiO<sub>2</sub> nanoparticle fabricated by a sol-gel process [98], and 3.26 eV for TiO<sub>2</sub> fabricated by a sol-gel process [95].

In the case of calcium titanate, 3.3 eV was measured for CaTiO<sub>3</sub> and 3.05–3.2 eV is calculated; Ca<sub>3</sub>Ti<sub>2</sub>O<sub>7</sub> and Ca<sub>4</sub>Ti<sub>3</sub>O<sub>10</sub> have identical values [94].

## 7.2. The passive film on Ti

Due to its non-stoichiometric composition, the passive film on Ti already contains oxygen defects. Consequently, the difference in the surface properties of passive films on Ti and TiO<sub>2</sub> ceramics is likely due to the difference in their  $E_g$ s. The  $E_g$  of passive films on Ti after anodic oxidation and thermal oxidation has been studied by the photoelectrochemical response in borate buffer solution, artificial sea water, and sulfuric acid [99–101], as conventional techniques for oxide ceramics, such as ultraviolet absorption, cannot be used for thin passive films on Ti. Nevertheless, the  $E_g$ s of the aforementioned study are  $3.25 \pm 0.05$  eV for the passive film on Ti anodically polarized in H<sub>2</sub>SO<sub>4</sub> [99,100], 3.4–3.7 eV for the passive film on Ti anodically polarized in sea water, and 3.1 eV in buffered solution [101]. Moreover, 3.4 and 3.7 eV after 400°C thermal oxidation [101]. However, the oxidation in these studies is excessive, and the passive films are converted to stable TiO<sub>2</sub> oxide.

Using the photoelectrochemical response at potentials as close as possible to the open-circuit potential, the  $E_g$  values of passive films formed on Ti in Hanks' solution and 0.9% NaCl aqueous solution have been evaluated recently [68]. The passive film on Ti behaved like an *n*-type semiconductor with two layers: an inner oxide layer with a high  $E_g$  and an outer hydroxide layer with a low  $E_g$ . In Hanks' solution, the value of  $E_g$  in the innermost layer was between 3.3 and 3.4 eV, whereas it was significantly lower in the surface layer (2.9 eV).  $E_g$  was 3.3 eV in the innermost layer and 2.7 eV in the outermost layer of saline. As

shown in Figure 13, the  $E_g$  values of the outermost surfaces of passive films formed on Ti (red circles) were much lower than those of TiO<sub>2</sub> ceramics [68]. Therefore, the passive film on Ti is more reactive than the ceramic TiO<sub>2</sub> surface. In addition to the excellent corrosion resistance, this reactivity likely contributes to the excellent biocompatibility of Ti. Calcium phosphate forms regularly on Ti, but not regularly on TiO<sub>2</sub>. The kinetics of calcium phosphate formation on Ti differ from those on TiO<sub>2</sub> crystalline ceramics [65].

## 7.3. ZrO<sub>2</sub> and the passive film on Zr

Zr is also a passive metal, whereas the passive film on Zr is a more stoichiometric oxide. ZrO<sub>2</sub> are well known as bioinert ceramics. Figure 12 also summarizes a portion of the published  $E_g$  data for ZrO<sub>2</sub> ceramics. The majority exceed the scale of the figure. Theoretical and experimental values are 5.2 eV and 6.5 eV in cubic, 5.2 eV and 6.0 eV in tetragonal, and 5.1 eV and 6.5 eV in monoclinic [102], and 3.26–4.97 eV in cubic, 4.07–4.99 eV in tetragonal, and 3.58–5.34 eV in monoclinic, according to a different study [103]. 5.55 eV for cubic, 6.40 eV for tetragonal, and 5.42 eV for monoclinic are theorized in another study [104]. In monoclinic, the theoretical value is 3.60 eV, while the experimental value is 5.8 eV [105]. Alternatively, experimental values of 5.0–5.8 eV are obtained [106–113]. In the case of ZrO<sub>2</sub> thin film deposition via sputtering, 4.52 eV is obtained [114]. In thin films of yttria-stabilized ZrO<sub>2</sub> (16% yttria),  $5.62 \pm 0.05$  eV [115]. In yttria-stabilized cubic ZrO<sub>2</sub>, 4.96 eV [116]. Therefore, ZrO<sub>2</sub> ceramics have significantly greater  $E_g$  than TiO<sub>2</sub> ceramics.

In the passive film on Zr, 4.44–4.91 eV in inner oxide layer and 3.01–3.47 eV in hydrated outer oxide layer and 4.3–5.7 eV [117]. 4.42–4.48 eV in Zr-5%(Nb; Mo; Ta; W) alloy [118]. The values are significantly greater than those of Ti.

Zr forms a highly stable and protective passive film, and its reactivity is much lower than that of Ti [84], as described in Section 6 above.  $E_g$  values for  $ZrO_2$  and passive films on Zr are significantly greater than those for  $TiO_2$  and passive films on Ti, respectively. This result is supporting that the reactivity of a substance can be determined using  $E_g$ .

#### 7.4. $Ta_2O_5$ and the passive film on Ta; $Nb_2O_5$ and the passive film on Nb

Ta and Nb are also known as passive metals. Ta and Nb are easily oxidized and passivated. Ta and Nb are popularly used for component elements of Ti alloys. Porous Ta is used as a bone defect filler and bone-contacting component in artificial joints. Additionally, Ta is utilized for skull implants and X-ray image markers for stents. Ta is ductile and produces excellent X-ray images due to the heavy metal [34]. Predominant compositions of the passive films are  $Ta_2O_5$  and  $Nb_2O_5$ , respectively [119]. As passive films,  $Ta_2O_5$  and  $Nb_2O_5$  are highly stable and resistant to corrosion in a biological environment.  $Ta_2O_5$  has potential applications in the electronic and catalytic industries.  $Nb_2O_5$  is used for catalysts and the production of optical glasses and lithium niobate for solar panel.

As depicted in Figure 12, the  $E_g$ s were 4.1 eV [120] and approximately 4 eV [121] for  $Ta_2O_5$ , 3.7 eV in the  $\gamma$  phase theory [122], and 4.1 eV for the passive film on Ta [123].

$E_g$ s of  $Nb_2O_5$  anodic oxidation film on Nb are 3.4 eV [121], 3.33–3.38 eV [124], 3.3 eV [125], 3.4 eV [126], and 3.77–3.85 eV [127]. The  $E_g$ s for  $Nb_2O_5$  nanoparticles are 3.05 eV nanoparticle [128], 3.72 eV for  $Nb_2O_5$  nanotubes and 3.97 eV for  $Nb_2O_5$  nanorods [129], and 3.16–4.19 eV for vapor-deposited  $Nb_2O_5$  thin films [130]. A review article states that the  $E_g$ s of  $Nb_2O_5$  are between 3.2 and 5 eV [131].

According to the preceding data, the  $E_g$ s of  $Ta_2O_5$  and  $Nb_2O_5$  are significantly greater than those of  $TiO_2$ . Therefore, the  $E_g$ s of the passive film on Ta and Nb are larger than that on Ti: The  $E_g$  of the passive film on Ti is lowest.

#### 7.5. $Cr_2O_3$ , $Fe_2O_3$ , and the passive film on stainless steels

$Cr_2O_3$  is the predominant component of passive films on stainless steels and Co–Cr alloys, while  $Fe_2O_3$  is sometimes present in passive films on stainless steels. As depicted in Figure 12, the  $E_g$  of  $Cr_2O_3$  nanoparticles varies depending on the firing temperature [132]. The  $E_g$  of  $Cr_2O_3$  has been calculated to be 3.4 eV [133]. The experimental value for  $Cr_2O_3$  is 3.4 eV, whereas the theoretical value for  $Fe_2O_3$  is 3.28–3.3 eV and the experimental value is 2.27 eV [134].

Therefore, the  $E_g$  of  $Cr_2O_3$  is comparable to that of  $TiO_2$  and that of  $Fe_2O_3$  is lower than that of  $TiO_2$ . The  $E_g$ s of the passive film on austenitic stainless steel type 316 L range between 2.00 and 3.40 eV [94] and  $1.95 \pm 0.5$  eV [135]. In addition, the outer Cr hydroxide layers of the passive film on Fe–Cr alloy have an  $E_g$  of 2.4 eV [136–140]. Consequently, the  $E_g$ s of the passive film on stainless steels is significantly lower than that on Ti. However, remember that the corrosion resistance of stainless steels is significantly lower than that of Ti.

#### 7.6. Relationship between band gap energy and reactivity

According to the review above, the  $E_g$ s of other oxides on passive metals are significantly larger than that of Ti. Therefore, Ti may exhibit optimal reactivity among passive metals, particularly in comparison to Zr. The optimal balance between high corrosion resistance and appropriate reactivity of Ti as a result of the passive oxide film is one of the most important reasons for the excellent biocompatibility of Ti among metals.

### 8. Conclusions

According to the above review and discussion of previous papers, it is possible to explain the excellent biocompatibility of Ti through the following considerations.

- The excellent corrosion resistance of Ti compared to other metals due to a macroscopically strong passive film.
- Ti ions are stabilized immediately to prevent toxicity if released into body fluids.
- Positive and negative charges are well-balanced due to the dissociation of surface hydroxyl groups on the passive film.
- Low electrostatic force of the passive film inducing a natural adsorption of proteins retaining their natural conformation.
- Excellent performance as an  $n$ -type semiconductor.
- Lower bandgap energy of the passive film on Ti produces optimal reactivity.
- As a result of this reaction, calcium phosphate is naturally formed.

It should be mentioned again that the optimal balance between high corrosion resistance and appropriate reactivity of Ti as a result of the passive oxide film is the most prevalent solution for excellent biocompatibility of Ti. The combination of these properties and the resulting biological response is essential to the elucidation of the biocompatibility of materials as a future spectacular subject. In future, this topic will



be essential to better understand the interface phenomena between materials and host bodies using materials informatics (MI) and materials digital transformation (Material DX), because all biological and tissue reactions start from an electronic transfer of the surface.

## Disclosure statement

No potential conflict of interest was reported by the author(s).

## Funding

This work was financially supported by the Design & Engineering by the Joint Inverse Innovation for Materials Architecture (DEJI<sup>2</sup>MA) Project and the Viable Materials Project, Ministry of Education, Culture, Sports, Science, and Technology (MEXT), Japan.

## Notes on contributor

**Takao Hanawa** is Professor of Department of Metallic Biomaterials, Institute of Biomaterials and Bioengineering (IBB), Tokyo Medical and Dental University (TMDU) since 2004. He also has positions as Professor of Center for Advanced Medical Engineering Research and Development, Kobe University, and Division of Materials and Manufacturing Science, Graduate School of Engineering, Osaka University. He is now a Council Member of the Science Council of Japan since 2020. He was once presidents of the Japanese Society for Biomaterials and Japanese Society for Dental Materials and Devices. He received his Ph.D. from Hokkaido University in 1989 and Tohoku University at 1998. He has experienced as Assistant Professor at Hokkaido University, Associate Professor at Tokushima University, and Deputy-in-General of Biomaterials Research Center, National Institute for Materials Science (NIMS). He has developed several surface treatment techniques and new metallic biomaterials. Recently, a micro-arc oxidation process to add dual-function to titanium and nano-topography to accelerate the differentiation of stem cells by femto-second laser, and zirconium alloys showing low magnetic susceptibility to decrease MRI artifact have been developed. In addition, interface reaction between titanium and living tissues is a life work of him.

## ORCID

Takao Hanawa  <http://orcid.org/0000-0003-1688-1749>

## References

- [1] Brunette DM, Tenvall P, Textor M, et al. Titanium in medicine. Berlin: Springer; 2001. DOI:10.1007/978-3-642-56486-4
- [2] Hanawa T. Titanium-Tissue interface reaction and its control with surface treatment. Front Bioeng Biotechnol. 2019;7:170.
- [3] Hanawa T. Zirconia versus titanium in dentistry: A review. Dent Mater J. 2020;39(1):24–36.

- [4] Tschernitschek H, Borchers L, Geurtsen W. Nonalloyed titanium as a bioinert metal—a review. J Prosth Dent. 2006;96(1):12.
- [5] William DF. Definitions in biomaterials. Proceedings of a Consensus Conference of the European Society for Biomaterials, Vol. 4, Chester, England, New York, NY: Elsevier; 1987.
- [6] Brånemark PI, Hansson BO, Adell R, et al. Osseointegrated implants in the treatment of the edentulous jaw. Experience from a 10-year period. Scand J Plasti Reconstr Surg Suppl. 1977;16:1–132.
- [7] Rupp F, Liang L, Geis-Gerstorf J, et al. Surface characteristics of dental implants: A review. Dent Mater. 2018;34(1):40–57.
- [8] Shah FA, Thomsen P, Palmquist A. A review of the impact of implant biomaterials on osteocytes. J Dent Res. 2018;97(9):977–986.
- [9] Shah FA, Thomsen P, Palmquist A. Osseointegration and current interpretations of bone-implant interface. Acta Biomater. 2019;84:1–15.
- [10] Sanderson PL, Ryan W, Turner PG. Complications of metalwork removal. Injury. 1992;23(1):29–30.
- [11] Speck KM, Fraker AC. Anodic polarization behavior of Ti-Ni and Ti-6Al-4V in simulated physiological solutions. J Dent Res. 1980;59(10):1590–1595.
- [12] Nakayama Y, Yamamuro T, Kumar P, et al. Anodic polarization measurements of orthopaedic implant alloys in bovine serum albumin. J Appl Biomater. 1990;1(4):307–313.
- [13] Nakayama Y, Yamamuro T, Kotoura Y, et al. In vivo measurement of anodic polarization of orthopaedic implant alloys: Comparative study of in vivo and in vitro experiments. Biomaterials. 1989;10(6):420–424.
- [14] Asri RIM, Harun WSW, Samykano M, et al. Corrosion and surface modification on biocompatible metals: A review. Mater Sci Eng C. 2017;77:1261–1274.
- [15] Manam NS, Harun WSW, Shri DNA, et al. Study of corrosion in biocompatible metals for implants: A review. J Alloy Compound. 2017;701:698–715.
- [16] Eliaz N. Corrosion of metallic biomaterials: A review. Materials. 2019;12(3):407.
- [17] Meachin G, Williams DF. Change in non-osseous tissue adjacent to titanium implants. J Biomed Mater Res. 1973;7:555–572.
- [18] Woodman JL, Jacobs JJ, Galante JO, et al. Metal ion release from titanium-based prosthetic segmental replacements of long bones in baboons: A long-term study. J Orthop Res. 1984;1(4):421–430.
- [19] Bessho K, Fujimura K, Iizuka T. Experimental long-term study of titanium ions eluted from pure titanium miniplates. J Biomed Mater Res. 1995;29(7):901–904.
- [20] Ektessabi AM, Otsuka T, Tsuboi Y, et al. Application of micro beam PIXE to detection of titanium ion release from dental and orthopaedic implants. Int J PIXE. 1994;4:81–91.
- [21] Ektessabi AM, Otsuka T, and Tsuboi Y, et al. Preliminary experimental results on mapping of the elemental distribution of organic tissues surrounding titanium-alloy implants. Nucl Instr Meth Phys Res B. 1996;109-110:278–283.
- [22] Bianco PD, Ducheyne P, Cuckler JM. Local accumulation of titanium released from a titanium implant in the absence of wear. J Biomed Mater Res. 1996;31:227–234.

- [23] Williams RL, Brown SA, Merritt K. Electrochemical studies on the influence of proteins on the corrosion of implant alloys. *Biomaterials*. 1988;9(2):181–186.
- [24] Clark GCF, Williams DF. The effects of proteins on metallic corrosion. *J Biomed Mater Res*. 1982;16(2):125–134.
- [25] Merritt K, Brown SA. Effect of proteins and pH on fretting corrosion and metal ion release. *J Biomed Mater Res*. 1988;22(2):111–120.
- [26] Bruneel N, Helsen JA. In vitro simulation of biocompatibility of Ti-Al-V. *J Biomed Mater Res*. 1988;22(3):203–214.
- [27] Ryhanen J, Niemi E, Serlo W, et al. Biocompatibility of nickel-titanium shape memory metal and its corrosion behaviour in human cell cultures. *J Biomed Mater Res*. 1997;35:451–457.
- [28] Hanawa T, Kohyama Y, Hiromoto S, et al. Effects of biological factors on the repassivation current of titanium. *Mater Trans*. 2004;45(5):1635–1639.
- [29] Tang L, Eaton JW. Fibrin(ogen) mediates acute inflammatory responses to biomaterials. *J Exp Med*. 1993;178(6):2147–2156.
- [30] Tengvall P, Lundström I, Sjöqvist L, et al. Titanium-Hydrogen peroxide interaction: Model studies of the influence of the inflammatory response on titanium implants. *Biomaterials*. 1989;10(3):166–175.
- [31] Pan J, Liao H, Leygraf C, et al. Variation of oxide films on titanium induced by osteoblast-like cell culture and the influence of an H<sub>2</sub>O<sub>2</sub> pretreatment. *J Biomed Mater Res*. 1998;40:244–256.
- [32] Mu Y, Kobayashi T, Sumita M, et al. Metal ion release from titanium with active oxygen species generated by rat macrophages in vitro. *J Biomed Mater Res*. 2000;49:238–243.
- [33] Mu Y, Kobayashi T, Tsuji K, et al. Causes of titanium release from plate and screws implanted in rabbits. *J Mater Sci Mater Med*. 2002;13(6):583–588.
- [34] Hanawa T. Overview of metals and applications. In: Duxford BNM, editor. *Metals for medical devices*. 2nd ed. UK: Wodhead; 2019. p. 3–30. DOI:10.1016/B978-0-08-102666-3.00001-8
- [35] Ilevbare GO, Burstein GT. The role of alloyed molybdenum in the inhibition of pitting corrosion in stainless steels. *Corros Sci*. 2001;43(3):485–513.
- [36] Akazawa T, Minami S, Takahashi K, et al. Corrosion of spinal implants retrieved from patients with scoliosis. *J Orthop Res*. 2005;10:200–205.
- [37] Tomizawa Y, Hanawa T, Kuroda D, et al. Corrosion of stainless sternal wire after long-term implantation. *J Artif Organ*. 2006;9(1):61–66.
- [38] Hiromoto S, Onodera E, Chiba A, et al. Microstructure and corrosion behaviour in biological environments of the new forged low-Ni Co–Cr–Mo alloys. *Biomaterials*. 2005;26(24):4912–4923.
- [39] Tsutsumi Y, Doi H, Nomura N, et al. Surface composition and corrosion resistance of Co–Cr alloys containing high chromium. *Mater Trans*. 2016;57(12):2033–2040.
- [40] Ikeda T, Takahashi K, Kabata T, et al. Polyneuropathy caused by cobalt–chromium metallosis after total hip replacement. *Muscle Nerve*. 2010;42(1):140–143.
- [41] Czekaj J, Ehlinger M, Rahme M, et al. Metallosis and cobalt – chrome intoxication after hip resurfacing arthroplasty. *Orthop Sci*. 2016;21(3):389–394.
- [42] Hallab NJ, Frank Chan FW, Harper ML. Quantifying subtle but persistent peri-spine inflammation in vivo to submicron cobalt–chromium alloy particles. *Europ Spine J*. 2012;21(12):2649–2658.
- [43] Hanawa T, Asami K, Hiromoto S. Characterization of the surface oxide film of a Co–Cr–Mo alloy after being located in quasi-biological environments using XPS. *Appl Surf Sci*. 2001;183(1–2):68–75.
- [44] Nagai A, Tsutsumi Y, Suzuki Y, et al. Characterization of air-formed surface oxide film on a Co–Ni–Cr–Mo alloy (MP35N) and its change in Hanks' solution. *Appl Surf Sci*. 2012;258(14):5490–5498.
- [45] Kocijan A, Milošev I, Pihlar B. Cobalt-Base alloys for orthopaedic applications studied by electrochemical and XPS analysis. *J Mater Sci Mater Med*. 2004;15(6):643–650.
- [46] Hiromoto S, Kano K, Suzuki Y, et al. Surface characterization and anodic polarization of nitrogen-ion-implanted Nickel-Free Co–Cr–Mo alloy. *Mater Trans*. 2005;46(7):1627–1632.
- [47] Milošev I, Strehblow HH. The composition of the surface passive film formed on CoCrMo alloy in simulated physiological solution. *Electrochim Acta*. 2002;48:2767–2774.
- [48] Maruyama N, Kawasaki H, Yamamoto A, et al. Friction-wear properties of Nickel-Free Co–Cr–Mo alloy in a simulated body fluid. *Mater Trans*. 2005;46(7):1588–1592.
- [49] Hanawa T, Nakazawa K, Kano K, et al. Friction-wear properties of Nitrogen-Ion-Implanted Nickel-Free Co–Cr–Mo alloy. *Mater Trans*. 2005;46(7):1593–1596.
- [50] Heintz C, Riepe G, Birken L, et al. Corroded nitinol wires in explanted aortic endografts: An important mechanism of failure? *J Endovasc Ther*. 2001;8(3):248–253.
- [51] Guidoin R, Marois Y, Douville Y, et al. First-Generation aortic endografts: analysis of explanted stentor devices from the EUROSTAR registry. *J Endovasc Ther*. 2000;7(2):105–122.
- [52] Chen P, Nagai A, Tsutsumi Y, et al. Differences in the calcification of preosteoblast cultured on sputter-deposited titanium, zirconium, and gold. *J Biomed Mater Res*. 2016;104A:639–651.
- [53] Itakura Y, Tajima T, Oho S, et al. Osteocompatibility of platinum-plated titanium assessed in vitro. *Biomaterials*. 1989;10(7):489–493.
- [54] Revie RW, Uhlig HH. *Corrosion and corrosion control: an introduction to corrosion science and engineering*. 4th ed. Berlin: Wiley; 2008. DOI:10.1002/9780470277270
- [55] Kelly EJ. Electrochemical behavior of titanium. *Mod Aspect Electrochem*. 1982;14:319–424.
- [56] Eda Y, Manaka T, Hanawa T, et al. X-Ray photoelectron spectroscopy-based valence band spectra of passive films on titanium. *Surf Interface Anal*. 2022;54(8):892–898.
- [57] Asami K, Chen SC, Habazaki H, et al. The surface characterization of titanium and titanium–nickel alloys in sulfuric acid. *Corros Sci*. 1993;35(1–4):43–49.
- [58] Silverman DC. Application of EMF–pH diagrams to corrosion prediction. *Corrosion*. 1982;38(10):541–549.
- [59] Olver JW, Ross JW. On the standard potential of the titanium(iii)–titanium(ii) couple. *J Am Chem Soc*. 1963;85(17):2565–2566.

- [60] Beck TR. Electrochemistry of freshly-generated titanium surfaces. I. Scraped-rotating-disk experiments. *Electrochim Acta*. 1973;18:807–814.
- [61] Asami K, Hashimoto K. The X-ray photo-electron spectra of several oxides of iron and chromium. *Corros Sci*. 1977;17(7):559–570.
- [62] Hanawa T, Asami K, Asaoka K. Repassivation of titanium and surface oxide film regenerated in simulated body fluid. *J Biomed Mater Res*. 1998;40:530–538.
- [63] Hiji A, Hanawa T, Shimabukuro M, et al. Initial formation kinetics of calcium phosphate on titanium in Hanks' solution characterized using XPS. *Surf Interface Anal*. 2021;53(2):185–193.
- [64] Wang L, Yu H, Wang K, et al. Local fine structural insight into mechanism of electrochemical passivation of titanium. *ACS Appl Mater Interfaces*. 2016;8(28):18608–18619. <https://doi.org/10.1021/acsami.6b05080>
- [65] Hiji A, Hanawa T, Yokoi T, et al. Time transient of calcium and phosphate ion adsorption by rutile crystal facets in Hanks' solution characterized by XPS. *Langmuir*. 2021;37(12):3597–3604.
- [66] Breeson AC, Sankar G, Goh GKL, et al. Phase quantification by X-ray photoemission valence band analysis applied to mixed phase TiO<sub>2</sub> powders. *Appl Surf Sci*. 2017;423:205–209.
- [67] Singh AP, Kodan N, Mehta BR. Enhancing the photoelectrochemical properties of titanium dioxide by thermal treatment in oxygen deficient environment. *Appl Surf Sci*. 2016;372:63–69.
- [68] Kim SC, Hanawa T, Manaka T, et al. Band structures of passive films on titanium in simulated body fluids determined by photoelectrochemical response: Principle governing the biocompatibility. *Sci Technol Adv Mater*. 2022;23(1):322–331.
- [69] Boehm HP. Functional groups on the surfaces of solids. *Angew Chem*. 1966;5(6):533–544.
- [70] Boehm HP. Acidic and basic properties of hydroxylated metal oxide surfaces. *Discuss Faraday Soc*. 1971;52:264–289.
- [71] Parfitt GD. The surface of titanium dioxide. *Prog Surf Membr Sci*. 1976;11:181–226.
- [72] Westall J, Hohl H. A comparison of electrostatic models for the oxide/solution interface. *Adv Colloid Interface Sci*. 1980;12(4):265–294.
- [73] Lide DR editor. CRC handbook of chemistry and physics. 87th ed. Boca Raton, FL: CRC Press; 2006. p. 6–2.
- [74] Sundgren JE, Bodö P, Ivarsson B, et al. Adsorption of fibrinogen on titanium and gold surfaces studied by ESCA and ellipsometry. *J Colloid Interface Sci*. 1986;113(2):530–543.
- [75] Hanawa T, Ota M. Calcium phosphate naturally formed on titanium in electrolyte solution. *Biomaterials*. 1991;12(8):767–774.
- [76] Hanawa T, Ota M. Characterization of surface film formed on titanium in electrolyte using XPS. *Appl Surf Sci*. 1992;55(4):269–276.
- [77] Healy KE, Ducheyne P. The mechanisms of passive dissolution of titanium in a model physiological environment. *J Biomed Mater Res*. 1992;26(3):319–338.
- [78] Serro AP, Fernandes AC, Saramago B, et al. Apatite deposition on titanium surfaces — the role of albumin adsorption. *Biomaterials*. 1997;18(14):963–968.
- [79] Frauchiger L, Taborelli M, Aronsson BO, et al. Ion adsorption on titanium surfaces exposed to a physiological solution. *Appl Surf Sci*. 1999;143(1–4):67–77.
- [80] Hiromoto S, Hanawa T, Asami K. Composition of surface oxide film of titanium with culturing murine fibroblasts L929. *Biomaterials*. 2004;25(6):979–986.
- [81] Sundgren JE, Bodo P, Lundstrom I. Auger electron spectroscopic studies of the interface between human tissue and implants of titanium and stainless steel. *J Colloid Interface Sci*. 1986;110(1):9–20.
- [82] Esposito M, Lausmaa J, Hirsch JM, et al. Surface analysis of failed oral titanium implants. *J Biomed Mater Res*. 1999;48(4):559–568.
- [83] Sundell G, Dahlin C, Andersson M, et al. The bone-implant interface of dental implants in humans on the atomic scale. *Acta Biomater*. 2017;48:445–450.
- [84] Tsutsumi Y, Nishimura D, Doi H, et al. Calcium phosphate formation on titanium and zirconium and its application to medical devices. *Mater Sci Eng C*. 2009;29:1702–1708.
- [85] Tsutsumi Y, Nishisaka T, Doi H, et al. Reaction of calcium and phosphate ions with titanium, zirconium, niobium, and tantalum. *Surf Interface Anal*. 2015;47(13):1148–1154.
- [86] Hodgson AWE, Mueller Y, Forster D, et al. Electrochemical characterisation of passive films on Ti alloys under simulated biological conditions. *Electrochim Acta*. 2002;47(12):1913–1923.
- [87] Chávez-Díaz MP, Luna-Sánchez R, Vazquez-Arenas J, et al. XPS and EIS studies to account for the passive behavior of the alloy Ti-6Al-4V in Hank's solution. *J Solid State Electrochem*. 2019;23(11):3187–3196.
- [88] Diebold U. The surface science of titanium dioxide. *Surf Sci Rep*. 2003;48:53–229.
- [89] Gao Q, Wu X, Fan Y, et al. Low temperature fabrication of nanoflower arrays of rutile TiO<sub>2</sub> on mica particles with enhanced photocatalytic activity. *J Alloy Comp*. 2013;579:322–329.
- [90] Yan M, Chen F, Zhang J, et al. Preparation of controllable crystalline titania and study on the photocatalytic properties. *J Phys Chem B*. 2005;109(18):8673–8678.
- [91] Stone JV, Davis RJ. Synthesis, characterization, and photocatalytic activity of titania and niobia mesoporous molecular sieves. *Chem Mater*. 1998;10(5):1468–1474.
- [92] Miao L, Tanemura S, Kondo Y, et al. Microstructure and bactericidal ability of photocatalytic TiO<sub>2</sub> thin films prepared by RF helicon magnetron sputtering. *Appl Surf Sci*. 2004;238(1–4):125–131.
- [93] Magnan H, Stanesco D, Rioult M, et al. Epitaxial TiO<sub>2</sub> thin film photoanodes: influence of crystallographic structure and substrate nature. *J Phys Chem C*. 2019;123(9):5240–5248.
- [94] Quarto FD, Zaffora A, Franco FD, et al. Critical review—photocurrent spectroscopy in corrosion and passivity studies: a critical assessment of the use of band gap value to estimate the oxide film composition. *J Electrochem Soc*. 2017;164(12):C671–C681.
- [95] Fonseca-Cervantes OR, Pérez-Larios A, Arellano VHR, et al. Effects in band gap for photocatalysis in TiO<sub>2</sub> support by adding gold and ruthenium. *Processes*. 2020;8(9):1032.



- [96] Kollbek K, Sikora M, Kapusta C, et al. X-Ray spectroscopic methods in the studies of nonstoichiometric  $\text{TiO}_{2-x}$  thin film. *Appl Surf Sci.* **2013**;281:100–104.
- [97] Ju Y, Li L, Wu Z, et al. Effect of oxygen partial pressure on the optical property of amorphous titanium oxide thin films. *Energy Proced.* **2011**;12:450–455.
- [98] Valencia S, Marín JM, Restrepo G. Study of the bandgap of synthesized titanium dioxide nanoparticles using the sol-gel method and a hydrothermal treatment. *Open Mater Sci J.* **2010**;4(2):9–14.
- [99] Di Quarto F, Piazza S, Sunseri C. The photoelectrochemistry of thin passive layers. Investigation of anodic oxide films on titanium metals. *Electrochim Acta.* **1993**;38(1):29–35.
- [100] Marsh J, Gorse D. A photoelectrochemical and ac impedance study of anodic titanium oxide films. *Electrochim Acta.* **1998**;43(7):659–670.
- [101] Kim DY, Kwon HS. A study on electronic properties of passive film formed on Ti. *Corros Sci Technol.* **2003**;2:212–218.
- [102] French RH, Glass SJ, Ohuchi FS, et al. Experimental and theoretical determination of the electronic structure and optical properties of three phases of  $\text{ZrO}_2$ . *Phys Rev B.* **1994**;49(8):5133–5142.
- [103] Jiang H, Gomez-Abal RI, Rinke P, et al. Electronic band structure of zirconia and hafnia polymorphs from the GW perspective. *Phys Rev B.* **2010**;81(8):085119.
- [104] Králík B, Chang EK, Louie SG. Structural properties and quasiparticle band structure of zirconia. *Phys Rev B.* **1998**;57(12):7027.
- [105] Li J, Meng S, Niu J, et al. Electronic structures and optical properties of monoclinic  $\text{ZrO}_2$  studied by first-principles local density approximation + U approach. *J Adv Ceram.* **2017**;6(1):43–49.
- [106] Sayan S, Bartynski RA, Zhao X, et al. Valence and conduction band offsets of a  $\text{ZrO}_2/\text{SiO}_x\text{N}_y/\text{n-Si}$  CMOS gate stack: a combined photoemission and inverse photoemission study. *Phys Status Solid B.* **2004**;241(10):2246–2252.
- [107] Bersch E, Rangan S, Bartynski RA, et al. Band offsets of ultrathin high- $\kappa$  oxide films with Si. *Phys Rev B.* **2008**;78(8):085114.
- [108] Puthenkovilakam R, Chang JP. Valence band structure and band alignment at the  $\text{ZrO}_2/\text{Si}$  interface. *Appl Phys Lett.* **2004**;84(8):1353.
- [109] Miyazaki S. Photoemission study of energy-band alignments and gap-state density distributions for high- $\kappa$  gate dielectrics. *J Vac Sci Technol B.* **2001**;19(6):2212.
- [110] Nohira H, Tsai W, Besling W, et al. Characterization of ALCVD- $\text{Al}_2\text{O}_3$  and  $\text{ZrO}_2$  layer using X-ray photoelectron spectroscopy. *J Non-Cryst Solid.* **2002**;303(1):83–87.
- [111] Ikarashi N, Manabe K. Electronic structure analysis of Zr silicate and Hf silicate films by using spatially resolved valence electron energy-loss spectroscopy. *J Appl Phys.* **2003**;94(1):480.
- [112] Balog M, Schieber M, Michiman M, et al. In situ formation of protective oxide scales as measured by their inhibiting effect on the high temperature hydrogen permeability of heat exchanger materials. *Thin Solid Film.* **1977**;41:247–255.
- [113] Zhu L, Fang Q, He G, et al. Spectroscopic ellipsometry characterization of  $\text{ZrO}_2$  thin films by nitrogen-assisted reactive magnetron sputtering. *Mater Sci Semicond Process.* **2006**;9(6):1025–1030.
- [114] Venkataraj S, Kappertz O, Weis H. Structural and optical properties of thin zirconium oxide films prepared by reactive direct current magnetron sputtering. *J Appl Phys.* **2002**;92(7):3599.
- [115] Kosacki I, Petrovsky V, Anderson HU. Band gap energy in nanocrystalline  $\text{ZrO}_2$ :16%Y thin films. *Appl Phys Lett.* **1999**;74(3):341.
- [116] PaiVermeker VR, Petelin AN, Crowne FJ, et al. Color-center-induced band gap shift in yttria-stabilized zirconia. *Phys Rev B.* **1989**;40(12):8555.
- [117] Kim BY, Park CJ, Kwon HS. Effect of niobium on electronic properties of passive films on zirconium alloys. *J Electroanal Chem.* **2005**;576:269–278.
- [118] Takahashi K, Uno M, Okui M, et al. Photoelectrochemical properties and band structure of oxide films on zirconium–transition metal alloys. *J Alloy Comp.* **2006**;421(1–2):3030–308.
- [119] Tanaka Y, Nakai M, Akahori T, et al. Characterization of air-formed surface oxide film on Ti–29Nb–13Ta–4.6Zr alloy surface using XPS and AES. *Corros Sci.* **2008**;50(8):2111–2116.
- [120] Di Franco E, Zampardi G, Santamaria M, et al. Characterization of the solid state properties of anodic oxides on magnetron sputtered Ta, Nb, and Ta–Nb alloys. *J Electrochem Soc.* **2012**;159:C33–C39.
- [121] Lee J, Lu W, Kioupakis E. Electronic properties of tantalum pentoxide polymorphs from first-principles calculations. *Appl Phys Lett.* **2014**;105(20):202108.
- [122] Hur JH. First principles study of the strain effect on band gap of  $\gamma$  phase  $\text{Ta}_2\text{O}_5$ . *Comp Mater Sci.* **2019**;164:17–21.
- [123] Silva RA, Walls M, Rondot B, et al. Electrochemical and microstructural studies of tantalum and its oxide films for biomedical applications in endovascular surgery. *J Mater Sci Mater Med.* **2002**;13(5):495–500.
- [124] Mickova I. Photoelectrochemical study of anodically formed oxide films on niobium surfaces. *Croat Chem Acta.* **2010**;83:113–120.
- [125] Arita M, Hayashi Y. Photoelectrochemical properties of anodic oxide film on niobium. *Mater Trans Jim.* **1994**;35(4):233–237.
- [126] Nozik AJ. Photoelectrochemistry: Applications to solar energy conversion. *Ann Rev Phys Chem.* **1978**;29(1):189–222.
- [127] Viet A, Jose R, Reddy M, et al.  $\text{Nb}_2\text{O}_5$  photoelectrodes for dye-sensitized solar cells: choice of the polymorph. *J Phys Chem.* **2010**;114:21795–21800.
- [128] Habibi MH, Mokhtari R. Novel sulfur-doped niobium pentoxide nanoparticles: Fabrication, characterization, visible light sensitization and redox charge transfer study. *J Sol-Gel Sci.* **2011**;59(2):352–357.
- [129] Liu J, Xue D, Li K. Single-Crystalline nanoporous  $\text{Nb}_2\text{O}_5$  nanotubes. *Nanoscale Res Lett.* **2011**;6(1):138.
- [130] Sathasivam S, Williamson BAD, Althabaiti SA, et al. Chemical vapor deposition synthesis and optical properties of  $\text{Nb}_2\text{O}_5$  thin films with hybrid functional theoretical insight into the band structure and band gaps. *ACS Appl Mater Interface.* **2017**;9(21):18031–18038.
- [131] Nunes BN, Lopes OF, Patrocinio AOT, et al. Recent advances in niobium-based materials for photocatalytic solar fuel production. *Catalysts.* **2020**;10(1):126.

- [132] Kamari HM, Al-Hada NM, Baqer AA, et al. Comprehensive study on morphological, structural and optical properties of  $\text{Cr}_2\text{O}_3$  nano particle and its antibacterial activities. *J Mater Sci Mater El.* **2019**;30(8):8035–8046.
- [133] Moore EA. First-Principles study of the mixed oxide  $\alpha\text{-FeCrO}_3$ . *Phys Rev B.* **2007**;76(19):195107.
- [134] Praveen CS, Timon V, Valant M. Electronic band gaps of ternary corundum solid solutions from  $\text{Fe}_2\text{O}_3\text{-Cr}_2\text{O}_3\text{-Al}_2\text{O}_3$  system for photocatalytic applications: A theoretical study. *Comp Mater Sci.* **2012**;55:192–198.
- [135] Sudesh TL, Wijesinghe L, Blackwood DJ. Electrochemical & optical characterisation of passive films on stainless steels. *J Phys Conf Ser.* **2006**;28:74–78.
- [136] Tsuchiya H, Fujimoto S. Semiconductor properties of passive films formed on sputter-deposited Fe-18cr alloy thin films with various additive elements. *Sci Technol Adv Mater.* **2004**;5:195–200.
- [137] Tsuchiya H, Fujimoto S, Chihara O, et al. Semiconductive behavior of passive films formed on pure Cr and Fe–Cr alloys in sulfuric acid solution. *Electrochim Acta.* **2002**;47(27):4357–4366.
- [138] Fujimoto S, Tsuchiya H. Semiconductor properties and protective roles of passive films of iron base alloys. *Corros Sci.* **2007**;49(1):195–202.
- [139] Tsuchiya H, Fujimoto S, Shibata T. Semiconductive properties of passive films formed on Fe-18cr in borate buffer solution. *J Electrochem Soc.* **2004**;151(2):B39–B44.
- [140] Tsuchiya H, Fujimoto S, Shibata T. Semiconductive properties of passive films formed on Fe–Cr alloy. *J Electroceram.* **2006**;16(1):49–54.